

## Use of Natural Rubber Membranes as Support for Powder $\text{TiO}_2$ and $\text{Ag}/\text{TiO}_2$ Photocatalysts

**Jusinei M. Stropa,<sup>a</sup> Aline S. Herrero,<sup>a</sup> Silvio C. Oliveira,<sup>a</sup> Alberto A. Cavalheiro,<sup>c</sup> Renato F. Dantas,<sup>d</sup> Samuel L. Oliveira,<sup>b</sup> Amilcar Machulek Jr.\*<sup>a</sup> and Lincoln C. S. Oliveira<sup>a</sup>**

<sup>a</sup>*Instituto de Química and <sup>b</sup>Instituto de Física, Universidade Federal de Mato Grosso do Sul, 79074-460 Campo Grande-MS, Brazil*

<sup>c</sup>*CPTREN, Universidade Estadual de Mato Grosso do Sul, 79950-000 Naviraí-MS, Brazil*

<sup>d</sup>*Escola de Tecnologia, Universidade de Campinas, UNICAMP, Paschoal Marmo 1888, 13484-332 Limeira-SP, Brazil*

The purpose of this study was to synthesize  $\text{TiO}_2$ -polymer composites able to act as photocatalyst membranes.  $\text{TiO}_2$  catalysts were prepared using the sol-gel method to contain 0.0, 0.5, 1.0, and 2.0 wt.% of embedded Ag particles, subsequently incorporated into natural rubber latex at a weight fraction of 15%. Samples of these ceramic powders were suspended in a latex emulsion (natural rubber), cast in Petri dishes and slowly dried in an oven. The resulting materials were evaluated by X-ray diffraction, scanning electron microscopy, energy-dispersive X-ray, diffuse reflectance spectroscopy, differential scanning calorimetry, thermogravimetry, and photocatalytic assaying using methylene blue as an organic pollutant reference. All composite membranes exhibited good photoactivity conferred by  $\text{TiO}_2$  powder, with 98% dye fading after 300 min of ultraviolet irradiation.

**Keywords:** titanium dioxide, silver, membrane, natural rubber, heterogeneous photocatalysis

### Introduction

Anatase-phase titanium dioxide ( $\text{TiO}_2$ ) is the most widely used semiconductor in water purification by heterogeneous photocatalysis, owing to characteristics such as photon efficiency, low cost, and absence of toxicity.<sup>1-5</sup> Photocatalytic reactions based on semiconductor excitation by high-energy radiation, such as ultraviolet (UV), are known to promote electrons ( $e^-$ ) from valence to conduction bands, leading to the appearance of holes ( $h^+$ ) in valence bands. Unrecombined electron-hole pairs subsequently migrate to the semiconductor surface, where they react with adsorbed substances through redox mechanisms.<sup>6</sup> In aqueous media, other species are indirectly formed, such as the hydroxyl radical ( $\text{HO}^\bullet$ ), a non-selective species that reacts with various organic molecules to yield  $\text{CO}_2$  and  $\text{H}_2\text{O}$ . Redox reactions involving the hydroxyl radical in aqueous media are termed advanced oxidation processes (AOPs).<sup>7-9</sup>

In recent decades, an increasing number of studies have been conducted to improve  $\text{TiO}_2$  performance by doping or modifying this material with other solid oxides or metallic elements.<sup>10-15</sup> Modifying  $\text{TiO}_2$  with noble metals enhances

its photocatalytic efficiency by promoting interfacial electron transfer, since these metals act as electron traps, delaying recombination of the electron-hole pair. Of all noble metals, silver has the lowest relative cost, making it the focus of most investigations and applications.<sup>16,17</sup> In addition, silver particles have been shown to exhibit biocidal properties against a number of microorganisms, another advantage of these silver-modified materials.<sup>18-20</sup>

Chemical approaches, including the sol-gel method, have been advantageously employed to produce silver-modified titanium dioxide ( $\text{Ag}/\text{TiO}_2$ ) for photocatalytic applications. This material can be obtained in a single step employing a metallic phase highly dispersed at the nanoscale, achieved using soluble precursors that facilitate the introduction of modifiers.<sup>21-23</sup> The sol-gel method is suitable for producing photocatalysts as reactive powders for use in aqueous suspensions or deposition of thin films on inert transparent substrates. However, the cost and complexity of separating reactive powders by ultrafiltration at the end of the process, coupled with the lack of flexibility of thin film supports, warrant the investigation of novel approaches.<sup>24-28</sup>

In the development of large-scale processes, composite structures are highly promising, especially polymer-based

\*e-mail: machulekjr@gmail.com

structures such as natural rubber.<sup>29-31</sup> According to Rippel and Galembeck,<sup>32</sup> “natural rubber is a strategic material, because it cannot be replaced by synthetic rubbers in some important applications, due to its outstanding elasticity, resilience, flexibility at low temperatures, resistance to abrasion, impact and corrosion, ready adhesion to textiles, steel, and to its impermeability, insulating properties, and ability to disperse heat. When compared to synthetic rubbers with similar performance, its price is often advantageous”.<sup>32</sup> These properties allow natural rubber to be shaped as desired and employed in the manufacture of countless types of products for use in a wide range of environments.<sup>33-38</sup>

This article reports the synthesis of Ag/TiO<sub>2</sub> photocatalysts employing the sol-gel method, as well as the immobilization of particulate material in natural rubber to obtain a second-generation composite of metallic, ceramic, and polymeric phases tailored to enhance photocatalytic performance in an aqueous medium.

## Experimental

### Reagents

All solutions were prepared in ultrapure distilled water. The following reagents were used: titanium IV isopropoxide (97%), nitric acid (65%), and methylene blue (82%), all from Sigma-Aldrich; isopropyl alcohol (PA, 99.5%), from Qhemis; silver nitrate (PA, 99.8%), from Synth; glacial acetic acid (99.7%), from F. Maia; ammonium hydroxide (PA, 98%), from Vetec; and pre-vulcanized latex suspension (60%), from Bassan.

### Synthesis of powder catalysts

Preparation of powder TiO<sub>2</sub> and Ag/TiO<sub>2</sub> catalysts using the sol-gel method<sup>24</sup> involved mixing titanium IV isopropoxide and glacial acetic acid at a molar ratio of 1:4 under constant stirring until formation of a metal acetate complex, followed by dilution with isopropyl alcohol at a 1:1 alcohol-to-alkoxide volumetric ratio. Stirring for 1 h was followed by addition of a stoichiometric amount of silver nitrate previously dissolved in water and acidified with drops of nitric acid to adjust pH ca. 2.0 (to avoid premature silver photoreduction), homogenization, and addition of water to achieve a 25:1 water-to-alkoxide molar ratio. The mixture was stirred for a further hour and left to jellify at room temperature for 24 h, after which the xerogel samples were dried at 100 °C for 24 h, ground in an agate mortar, and calcined in a muffle furnace at 450 °C for 4 h under a static air atmosphere. Four TiO<sub>2</sub> samples were

prepared to contain theoretical amounts of 0.0, 0.5, 1.0, and 2.0 wt.% of dispersed metallic silver nuclei. The samples were labeled TA00, TA05, TA10, and TA20, respectively.

### Synthesis of impregnated membranes

The powder catalysts were impregnated in natural rubber membranes using the casting method<sup>39</sup> to obtain dried membranes of approximately 3.0 g (natural rubber + catalyst). To adjust membrane coverage with the least possible amount of catalyst, several powder-to-polymer ratios were tested (5, 10, 15, 20, 30, and 50 wt.%). Because the best results were achieved with the sample containing 15 wt.% of ceramic powder, this ratio was adopted to produce all modified membranes, as follows.

First, each catalyst was crushed in an agate mortar and placed in a beaker containing 15 mL of ammonium hydroxide (10% m/v). The suspension was stirred for 10 min to ensure particle suspension and to prevent premature latex clotting. Pre-vulcanized latex (60%) was poured into the suspension, which was stirred for another 15 min, spread in Petri dishes (9 cm internal diameter), and dried in an oven at 50 °C for roughly 15 h. The membranes were named according to the catalysts employed in their composition, as follows: NRTA00, NRTA05, NRTA10, and NRTA20. One membrane prepared with bare natural rubber (labelled NRC) served as a control.

### Characterization of samples

Structural characterization of ceramic powders was performed by X-ray diffraction (XRD) on a D/MAX-2100/PC diffractometer (Rigaku) using Cu-K<sub>α</sub> radiation (40 kV, 120 mA), an iron filter for K<sub>β</sub> radiation, and slits for 0.5° divergence (5 mm aperture) and 0.5° scattering (0.3 mm aperture). A vertical goniometer was used in fixed time mode, at 0.02° steps and 1 s collection time at each angle, with 2θ/θ scans in the 10° to 80° range. Rietveld refinement (DBWS-9807 software) was performed using XRD raw data to determine structural parameters by comparison with the XRD profile found in JCPDS card number 21-1272 and with the atomic positions in ICSD card number 20-2242.<sup>40-43</sup> For morphological characterization, the samples were held on carbon tape, sputter-coated with gold under high vacuum, and observed by scanning electron microscopy (SEM) using a JEOL JSM-6380 LV microscope operating at 20 kV for surface scanning and energy dispersive X-ray analysis (EDX) and at 15 or 30 kV for cross-section scanning. The results obtained by XRD and EDX were treated for visualization using Origin software, version 6.0 (Microcal).

The optical properties of the ceramic powders were investigated by diffuse reflectance spectroscopy (DRS) on a USB4000 detector with a PX2 pulsed xenon lamp (both from Ocean Optics) connected by a bifurcated optical fiber and employing barium sulfate ( $\text{BaSO}_4$ ) as the standard for total diffuse reflectance in the 200–800 nm wavelength range. Raw reflectance and converted absorbance data were treated using Spectra Suite software (Ocean Optics).

Thermal properties were investigated by thermogravimetry (TG) and differential scanning calorimetry (DSC). TG measurements were performed on a TGA-Q50 thermobalance (TA Instruments) at a heating rate of  $10\text{ }^\circ\text{C min}^{-1}$  from 25 to  $800\text{ }^\circ\text{C}$  in an oxidizing synthetic air atmosphere at a  $60\text{ mL min}^{-1}$  flow, employing a platinum crucible as the support. DSC was performed on a DSC-Q20 calorimeter (TA Instruments) at a heating rate of  $10\text{ }^\circ\text{C min}^{-1}$  under a nitrogen atmosphere at a  $50\text{ mL min}^{-1}$  flow, using a standard TZero aluminum crucible (TA Instruments) with a crimped lid. A similar crucible was used as the reference. TG and DSC data were treated using Universal Analysis 2000 software, version 3.7 A (TA Instruments).

#### Photocatalytic assays

The membranes were evaluated for photocatalytic performance using an aqueous solution of methylene blue as a model pollutant.<sup>44</sup> A photoreactor equipped with an 80 W HPL-N high-pressure mercury vapor lamp (Phillips, 3600 lm nominal luminous flux,  $44.5\text{ lm W}^{-1}$  nominal luminous efficacy) was housed in a jacketed quartz tube for circulation of thermostated water at  $30 \pm 3\text{ }^\circ\text{C}$ .<sup>19-21</sup> This quartz tube was horizontally positioned 12 cm above the Petri dish (14 cm in diameter) containing 100 mL of methylene blue aqueous solution adjusted for an initial pH of close to 7.0 (Figure 1a). The initial dye concentration of  $0.01\text{ g L}^{-1}$  ( $3.13 \times 10^{-5}\text{ mol L}^{-1}$ ) corresponded to roughly 6 ppm of dissolved organic carbon. Each dye solution was evaluated once at room temperature ( $33 \pm 3\text{ }^\circ\text{C}$ ) during the entire experiment.

A circular portion was cut from the center of each membrane to facilitate spinning of the magnetic stirrer bar (Figure 1b). To ensure submersion, the membranes were adhered to the Petri dish with a small amount of raw latex. Adsorption equilibrium was reached by stirring for 30 min in the dark at room temperature before the lamp was turned on.<sup>45</sup> Dye fading was monitored at room temperature by UV-Vis spectrophotometry at 0, 30, 60, 90, 120, 180, 240, and 300 min. For comparison with photocatalysis results, the influence of photolysis (with the lamp as the only radiation source) on dye degradation was also investigated in the absence of membranes. The assemblage was kept in

a closed environment to minimize interference. Monitoring dye degradation in the photocatalysis and photolysis assays involved UV-Vis spectroscopy on a U-3000 UV-Vis spectrophotometer (Hitachi). The data obtained were treated using Origin software, version 6.0 (Microcal).

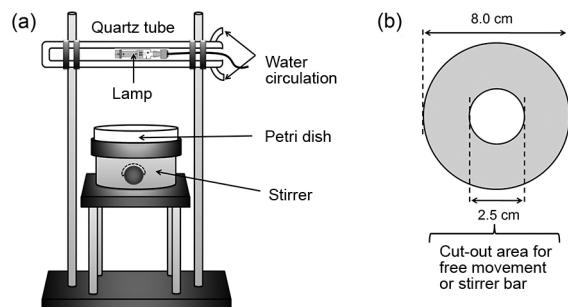


**Figure 1.** Reactor setup for photocatalytic assay in (a) and shape and dimensions of membranes used in the photocatalytic assays in (b).

## Results and Discussion

#### Characterization of powder catalysts

For all samples, XRD patterns (Figure 2) revealed a predominance of a single highly ordered anatase phase. Other  $\text{TiO}_2$  phases, such as rutile, are not relevant for photocatalysis. All anatase phase peaks were identified and marked in Figure 2 at  $25^\circ$ ,  $38^\circ$ ,  $48^\circ$ ,  $54^\circ$ ,  $55^\circ$ ,  $63^\circ$ ,  $69^\circ$ ,  $70^\circ$ , and  $74^\circ$  ( $\theta$ ), corresponding to (101), (004), (200), (105), (211), (204), (116), (220), and (107) diffraction planes ( $hkl$ ), respectively, taking into account the  $\text{TiO}_2$  anatase phase reported in the Joint Committee on Powder Diffraction Standards (JCPDS) databank (card number 21-1272).<sup>46,47</sup> No evidence was available of peaks related to nanocrystalline silver, probably because metallic silver particles are dispersed at the nanoscale in the ceramic matrix.

Full width at half maximum (FWHM) values obtained by Rietveld refinement (Table 1) were used for crystallite size calculation based on Scherrer's formula (equation 1), where  $D$  is the crystallite size;  $K$  is a constant with a typical value of 0.9;  $\lambda$  is the X-ray wavelength employed ( $\text{Cu}-\text{K}_{\alpha} = 0.15406\text{ nm}$ );  $\beta_c$  and  $\beta_s$  are the peak widths at half height (in rad) of the sample and standard (tungsten carbide, WC), respectively; and  $\theta$  is the Bragg angle of the most intense peak.

$$D = \frac{K\lambda}{(\beta_c - \beta_s)\cos\theta} \quad (1)$$

Table 2 shows the values obtained for crystallite sizes. Note that crystallite size increases as a function of silver amount, revealing that this metal assists in the

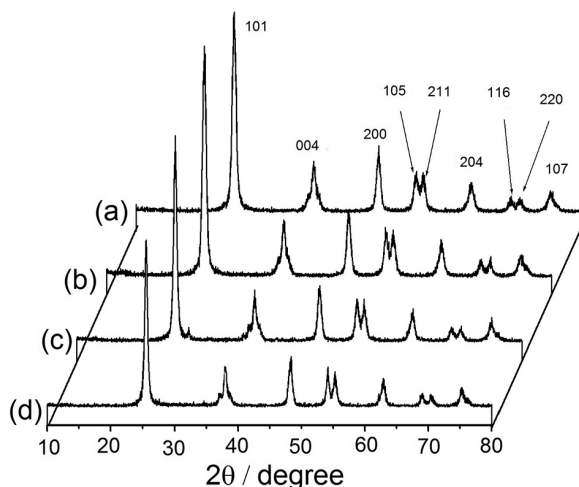


**Figure 2.** XRD patterns for (a) TA00; (b) TA05; (c) TA10; and (d) TA20 powder samples calcined at 450 °C for 4 h.

crystallinity of TiO<sub>2</sub> by favoring crystal ordering. This fact is corroborated by the FWHM values, which exhibit peak narrowing. The absence of defects in the crystal lattice is an important factor in the photocatalytic process, since these defects may act as recombination centers for charge carriers, leading to annihilation of the electron-hole pair.<sup>48,49</sup>

Band gap energy ( $E_g$ ) values were obtained by DRS analysis, in which reflectance data were converted into absorbance data using the software (Spectra Suite, by Ocean Optics) provided with the equipment. To calculate  $E_g$ , a tangent is drawn to the absorption edge in the region of maximum slope, revealing the characteristic wavelength ( $\lambda$ ) of the semiconductor (absorbance = 0). By substituting this value in equation 2,  $E_g$  is obtained.<sup>50-54</sup>  $E_g$  values are shown in Table 1, where  $h$  is Planck's constant and  $c$  is the speed of light in a vacuum. Note that  $E_g$  decreases slightly as a function of silver content, which seems to depend on anatase phase ordering, according to crystallite size.

$$E_g = \frac{hc}{\lambda} = \frac{1240 \text{ (eV nm)}}{\lambda \text{ (nm)}} \quad (2)$$

The absorbance *versus* wavelength curves (Figure 3) show tangent extrapolation, revealing the characteristic wavelengths of catalysts. Absorption is more evident in samples TA10 and TA20, involving surface plasmon

resonance of silver particles.<sup>55-58</sup> However, the intrinsic absorbance of TiO<sub>2</sub> is not necessarily affected, as revealed by the maintenance of a pattern that starts at around 400 nm.

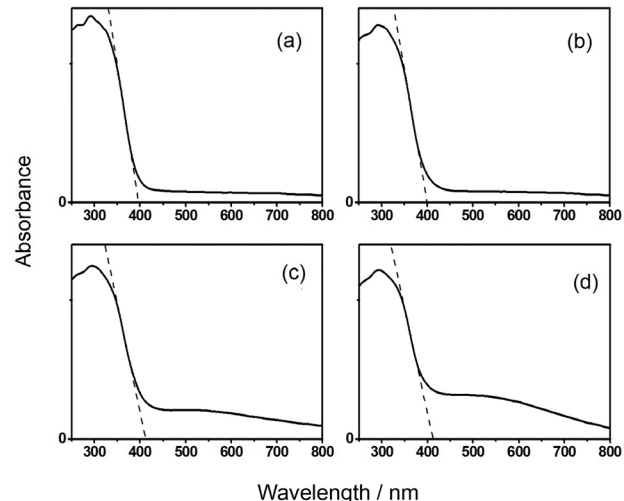


**Figure 3.** Diffuse reflectance spectroscopy curves and  $E_g$  values for (a) TA00; (b) TA05; (c) TA10; and (d) TA20 powder samples calcined at 450 °C for 4 h.

Irregular, nanometric particles can be seen in the SEM images (Figure 4) of all catalysts, agglomerating into larger, block-like irregular particles at the micrometric scale. According to the images, the amount of added silver does not appear to influence particle morphology or size. Moreover, the images provide no evidence of the presence of silver on the catalyst surfaces.

The presence of silver in the modified TiO<sub>2</sub> was confirmed by EDX analysis. In Figure 5, silver peaks can be observed in the inset, with differences in silver amounts translating to differences in intensity. The gold peaks shown in the inset represent gold coating (required for SEM analysis).

Cross-sectional micrographs (Figures 6b-6e) reveal phase separation for modified membranes (compared to the NRC membrane, Figure 6a), with a predominance of ceramic phase accumulating at the bottom as a result of sedimentation of ceramic material in the rubber solution during the drying step. This morphology favors their potential use as photocatalysts, because the accumulation

**Table 1.** FWHM values, diffraction angles, crystallite sizes, characteristic wavelengths, and band gap energies of the catalyst samples investigated

Sample	FWHM	Diffraction angle / degree	Crystallite size / nm	Characteristic wavelength / nm	$E_g$ / eV
TA00	0.700	25.36	18	400	3.1
TA05	0.680	25.32	19	400	3.1
TA10	0.610	25.41	23	410	3.0
TA20	0.540	25.46	28	410	3.0

FWHM: Full width at half maximum.

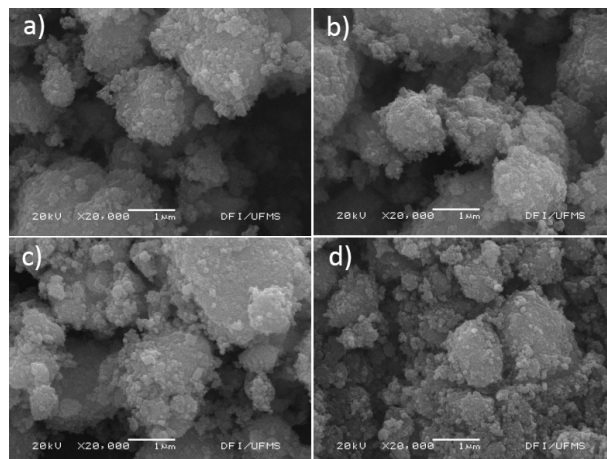


**Figure 4.** SEM images of (a) TA00; (b) TA05; (c) TA10; and (d) TA20 powder samples calcined at 450 °C for 4 h.

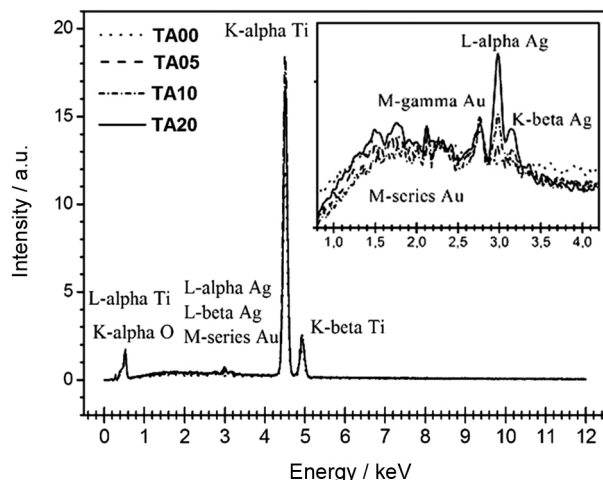


**Figure 5.** EDX spectrometry for powder samples calcined at 450 °C for 4 h.

of ceramic material on one side allows activation by light, triggering photocatalysis on the surface. Figure 7a shows the low rugosity of the NRC surface, relative to modified membranes. Note that many catalyst particles are exposed (Figures 7b–7e), arrested by the polymer network and remaining strongly adhered to the membranes, which prevents leaching and dispenses with the need for filtration at the end of the process.

The membrane TG curves virtually overlapped in the portions corresponding to the first mass loss from thermal decomposition, indicating that the catalysts did not significantly influence rubber thermal stability (Figure 8). The initial temperatures of mass loss for each membrane were calculated using Onset Point software (Table 2). The TG curves revealed different residue contents for pure and modified membranes, of roughly 1% and 16%, respectively, a difference (of around 15%) reflecting the amount of added catalyst.

DSC curves revealed glass transition temperatures ( $T_g$ )

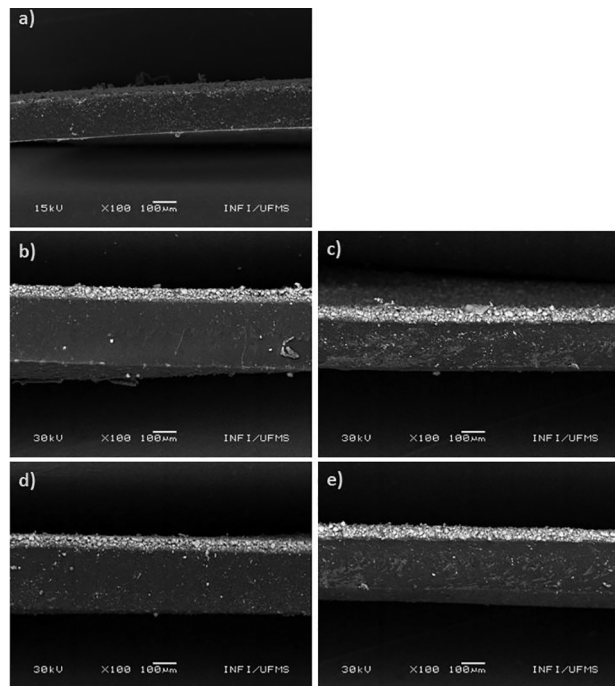


**Figure 6.** Cross-sectional SEM images of ceramic–rubber interfaces in (a) NRC; (b) NRTA00; (c) NRTA05; (d) NRTA10; and (e) NRTA20 membranes.

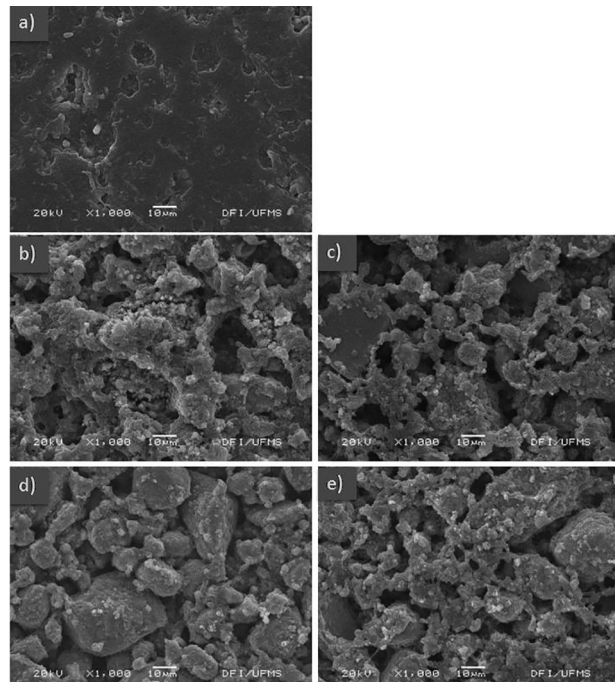


**Figure 7.** SEM images of (a) NRC; (b) NRTA00; (c) NRTA05; (d) NRTA10; and (e) NRTA20 membranes.

of about 64 °C for all membranes (Figure 9), as calculated using Onset Point software. This result indicates that the physical properties of rubber were preserved, as were characteristics of interest such as flexibility and elasticity.<sup>59</sup> These features make these materials good candidates for further investigation.

**Table 2.** Mass loss temperatures (calculated with Onset Point software) and residues obtained for bare (NRC) and catalyst-enriched membranes (NRTA00, NRTA05, NRTA10, NRTA20)

Membrane	NRC	NRTA00	NRTA05	NRTA10	NRTA20
Temperature of mass loss / °C	306.15	297.00	303.32	303.08	303.15
Residue / %	1.55	16.36	15.10	16.67	16.22

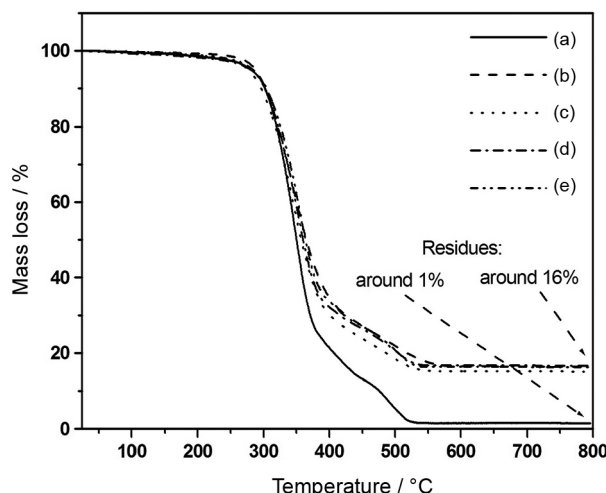


**Figure 8.** Thermogravimetric curves revealing thermal decomposition in (a) NRC; (b) NRTA00; (c) NRTA05; (d) NRTA10; and (e) NRTA20 membranes.

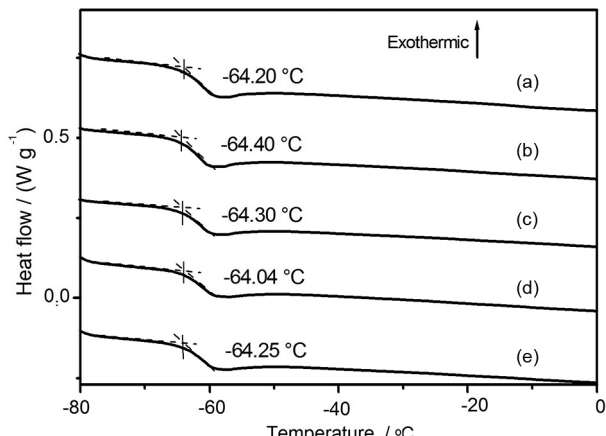


**Figure 9.** Differential scanning calorimetric curves showing glass transition temperatures (in the vicinity of -64 °C) for (a) NRC; (b) NRTA00; (c) NRTA05; (d) NRTA10; and (e) NRTA20 membranes.

### Photocatalysis employing membranes

The results of assays performed with rubber-supported photocatalysts are depicted as normalized curves corresponding to degradation ( $C/C_0$ ) as a function of time (Figure 10a).<sup>60</sup> The values of normalized concentrations were converted to degradation percentages using equation 3.

$$\text{Degradation (\%)} = \left( 1 - \frac{C}{C_0} \right) \quad (3)$$

Total methylene blue degradation by photocatalytic activity at 300 min was approximately 98% for all modified membranes, in contrast with 20% degradation by NRC and 14% by photolysis alone (Figure 10b). Promising results were obtained for all modified membranes, and variations in silver content did not appear to influence dye fading. Since natural rubber was not found to suppress photocatalytic activity, the materials investigated can be viewed as potential contributors furthering the development of coatings applied in heterogeneous photocatalysis.

The kinetics of methylene blue degradation were investigated using the Langmuir-Hinshelwood kinetics equation (equation 4) for a first-order reaction, where  $C_0$  is the initial concentration of dye,  $C$  is the concentration at time  $t$ , and  $k$  is the rate constant.<sup>61-63</sup>

$$\ln\left(\frac{C}{C_0}\right) = kt \quad (4)$$

According to this law, only a first-order reaction can generate a straight line when  $\ln(C_0/C)$  is plotted against  $t$ .<sup>64,65</sup> The approximate rate constant values calculated for the modified membranes are shown in Table 3. Results obtained for photolysis and the NRC membrane were not significant, and hence omitted. Figure 11 shows virtually straight lines for all modified membranes, with correlation coefficients ( $R$ ) close to 0.990, calculated using the first-order kinetic model (equation 4). The results compiled in Table 3 suggest that the presence of silver does not play an important role in the photocatalytic process taking place in the membranes, since all TiO<sub>2</sub> powder samples produced ceramic polymer composites that exhibited high photocatalytic performance. However, a biocide assay will be performed in an upcoming investigation in order to verify whether the amount of silver influences membrane functionality.

### Conclusions

The sol-gel method proved effective for producing catalysts with nanometric single-anatase-phase particles, which facilitates dispersion of the ceramic phase in natural rubber. Thermal stability of natural rubber membranes was not affected by the catalysts investigated. The chemical

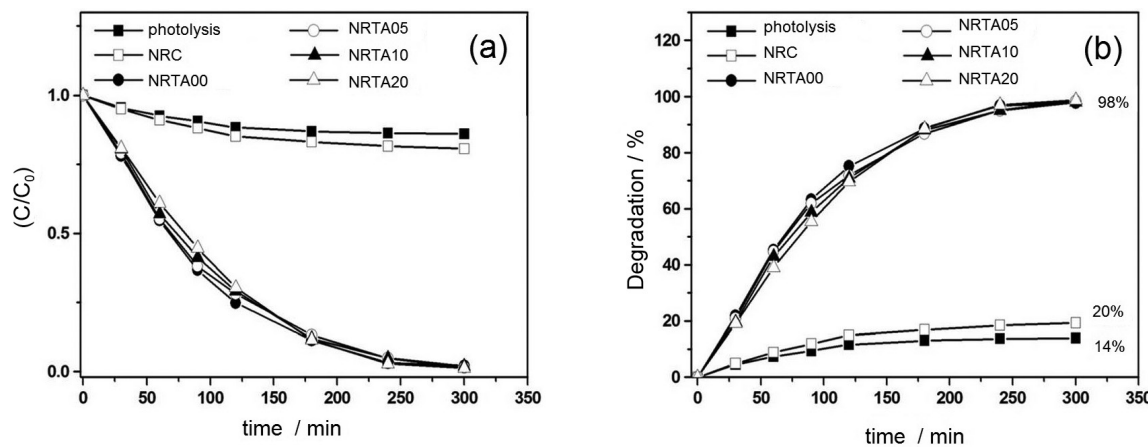


**Figure 10.** Methylene blue degradation by photocatalysis in the presence of bare and catalyst-enriched membranes, expressed as  $C/C_0$  ratios (a); and percentages (b).

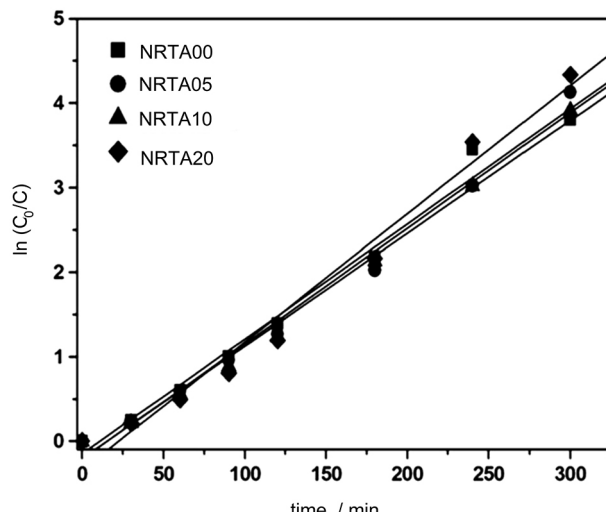


**Figure 11.** Kinetics of methylene blue degradation in the presence of catalyst-enriched membranes.

**Table 3.** Correlation coefficients ( $R$ ) and rate constants ( $k$ ) obtained for modified membranes by plotting  $\ln(C_0/C)$  versus time

Membrane	NRTA00	NRTA05	NRTA10	NRTA20
$R$	0.99356	0.99363	0.99635	0.98933
$k / \text{min}^{-1}$	$1.36 \times 10^{-2}$	$1.37 \times 10^{-2}$	$1.33 \times 10^{-2}$	$1.52 \times 10^{-2}$

characteristics of rubber were retained, as shown by stable TG values in the vicinity of  $-64^\circ\text{C}$ , indicating that elasticity and flexibility were preserved. These results suggest that no chemical interaction takes place between catalyst and rubber. All modified membranes exhibited photocatalytic ability, since 98% of the methylene blue present in the solution was degraded within 300 min, regardless of silver amount. This outcome was aided by a favorable morphology in which the catalyst was concentrated on one side of the membrane surface, facilitating activation by light. Photocatalytic degradation of methylene blue

using the modified membranes was considerably more pronounced than degradation using photolysis alone or with the NRC membrane, indicating activity of catalysts at the rubber surface. These results revealed the occurrence of synergy between catalyst and rubber properties, suggesting that the materials investigated have potential utility in the development of photocatalytic coatings.

## Acknowledgments

The authors wish to thank the Brazilian funding agencies Conselho Nacional de Desenvolvimento Científico e Tecnológico (CNPq), Coordenação de Aperfeiçoamento de Pessoal de Nível Superior (CAPES), and Fundação de Apoio ao Desenvolvimento do Ensino, Ciência e Tecnologia do Estado de Mato Grosso do Sul (Fundect) for their financial support. A. M. Jr. is associated with the Universidade de São Paulo Research Consortium for Photochemical Technology (NAP-Photo Tech) and the Instituto Nacional de Ciência e Tecnologia de Estudos do Meio Ambiente (INCT-EMA).

## References

- Henderson, M. A.; *Surf. Sci. Rep.* **2011**, *66*, 185.
- Hashimoto, K.; Irie, H.; Fujishima, A.; *Jpn. J. Appl. Phys.* **2005**, *44*, 8269.
- Chong, M. N.; Jin, B.; Chow, C. W. K.; Saint, C.; *Water Res.* **2010**, *44*, 2997.
- Ibhadon, A. O.; Fitzpatrick, P.; *Catalysts* **2013**, *3*, 189.
- Wankhade Atul, V.; Gaikwad, G. S.; Dhone, M. G.; Khaty, N. T.; Thakare, S. R.; *Res. J. Chem. Environ.* **2013**, *17*, 84.
- Zhang, W.; Li, Y.; Wang, C.; Wang, P.; Wang, Q.; *Water Res.* **2013**, *47*, 1480.
- Cavalcante, R. P.; Sandim, L. R.; Bogo, D.; Barbosa, A. M. J.; Osugi, M. E.; Blanco, M.; Oliveira, S. C.; Matos, M. F. C.;

- Machulek, A.; Ferreira, V. S.; *Environ. Sci. Pollut. Res.* **2013**, *20*, 2352.
8. Machulek, A.; Moraes, J. E. F.; Silverio, C. A.; Okano, L. T.; Quina, F. H.; *Photochem. Photobiol. Sci.* **2009**, *8*, 985.
9. Gozzi, F.; Machulek, A.; Ferreira, V. S.; Osugi, M. E.; Santos, A. P. F.; Nogueira, J. A.; Dantas, R. F.; Esplugas, S.; Oliveira, S. C.; *Chem. Eng. J.* **2012**, *210*, 444.
10. Yang, J.; Zhang, X.; Liu, H.; Wang, C.; Liu, S.; Sun, P.; Wang, L.; Liu, Y.; *Catal. Today* **2013**, *201*, 195.
11. Naldonia, A.; D'Arienzo, M.; Altomare, M.; Marelli, M.; Scotti, R.; Morazzoni, F.; Sellì, E.; Dal Santo, V.; *Appl. Catal., B* **2013**, *130*, 239.
12. Niu, Y.; Xing, M.; Zhang, J.; Tian, B.; *Catal. Today* **2013**, *201*, 159.
13. Chen, S. F.; Li, J. P.; Qian, K.; Xu, W. P.; Lu, Y.; Huang, W. X.; Yu, S. H.; *Nano Res.* **2010**, *3*, 244.
14. Pelaez, M.; Nolan, N. T.; Pillai, S. C.; Seery, M. K.; Falaras, P.; Kontos, A. G.; Dunlop, P. S. M.; Hamilton, J. W. J.; Byrne, J.; O'Shea, K.; Entezari, M. H.; Dionysiou, D. D.; *Appl. Catal., B* **2012**, *125*, 331.
15. Gegova, R.; Dimitriev, Y.; Bachvarova-Nedelcheva, A.; Iordanova, R.; Loukanov, A.; Iliev, T.; *J. Chem. Technol. Metall.* **2013**, *48*, 147.
16. Suwanchawalit, C.; Wongnawa, S.; Sriprang, P.; Meanha, P.; *Ceram. Int.* **2012**, *38*, 5201.
17. Yang, H.; Chen, F.; Jiao, Y.; Zhang, J.; *Appl. Catal., B* **2013**, *130*, 218.
18. Liu, Y.; Wang, X.; Yang, F.; Yang, X.; *Microporous Mesoporous Mater.* **2008**, *114*, 431.
19. Amin, S. A.; Pazouki, M.; Hosseinnia, A.; *Powder Technol.* **2009**, *196*, 241.
20. Dallas, P.; Sharma, V. K.; Zboril, R.; *Adv. Colloid Interface Sci.* **2011**, *166*, 119.
21. Mackenzie, J. D.; *J. Non-Cryst. Solids* **1988**, *100*, 162.
22. Dimitriev, Y.; Ivanova, Y.; Iordanova, R.; *J. Chem. Technol. Metall.* **2008**, *43*, 181.
23. Harraz, F. A.; Abdel-Salamb, O. E.; Mostafac, A. A.; Mohameda, R. M.; Hanafy, M.; *J. Alloy Compd.* **2013**, *551*, 1.
24. Cavalheiro, A. A.; Bruno, J. C.; Saeki, M. J.; Valente, J. P. S.; Florentino, A. O.; *Thin Solid Films* **2008**, *516*, 6240.
25. Liang, W.; Li, J.; Jin, Y.; *Building and Environment* **2012**, *51*, 345.
26. Viana, M. M.; Mohallem, N. D. S.; Miquita, D. R.; Balzuweit, K.; Silva-Pinto, E.; *Appl. Surf. Sci.* **2013**, *265*, 130.
27. Adams, M.; Skillen, N.; McCullagh, C.; Robertson, P. K. J.; *Appl. Catal., B* **2013**, *130*, 99.
28. Santos, V. P.; Carabineiro, S. A. C.; Tavares, P. B.; Pereira, M. F. R.; Orfao, J. J. M.; Figueiredo, J. L.; *Appl. Catal., B* **2010**, *99*, 198.
29. Ali, A.; Hosseini, M.; Sahari, B. B.; *Am. J. Eng. Appl. Sci.* **2010**, *1*, 232.
30. Dall'Antonia, A. C.; Martins, M. A.; Moreno, R. M. B.; Mattoso, L. H. C.; Job, A. E.; Ferreira, F. C.; Gonçalves, P. S.; *Polim.: Cienc. Tecnol.* **2006**, *3*, 239.
31. Mark, J. E.; *J. Chem. Educ.* **1981**, *11*, 898.
32. Rippel, M. M.; Galembeck, F.; *J. Braz. Chem. Soc.* **2009**, *20*, 1024.
33. van Beilen, J. B.; Poirier, Y.; *Trends in Biotechnol.* **2007**, *25*, 522.
34. Mooibroek, H.; Cornish, K.; *Appl. Microbiol. Biotechnol.* **2000**, *53*, 355.
35. Lakshmi, S.; Renganathan, R.; Fujita, S.; *J. Photochem. Photobiol. A* **1995**, *88*, 163.
36. Ramaswamy, V.; *Mater. Res. Bull.* **2008**, *43*, 1145.
37. Chin, S.; Park, E.; Kim, M.; Jurng, J.; *Powder Technol.* **2010**, *201*, 171.
38. Ogino, C.; Dadjour, M. F.; Iida, Y.; Shimizu, N.; *J. Hazard. Mater.* **2008**, *153*, 551.
39. Rao, V.; Johns, J.; *J. Appl. Polym. Sci.* **2008**, *107*, 2217.
40. Rietveld, H. M.; *J. Appl. Cryst.* **1969**, *2*, 65.
41. Young, R. A.; Larson, A. C.; Paiva-Santos, C. O.; *User's Guide to Program DBWS-9807 for Rietveld Analysis of X-ray and Neutron Powder Diffraction Patterns v. GA 30332*; School of Physics, Georgia Institute of Technology: Atlanta, 1998.
42. Joint Committee on Powder Diffraction Standards (JCPDS), International Center for Diffraction Data; *Powder File Card No. 21-1272*; JCPDS: Philadelphia, 2003.
43. Inorganic Crystal Structure Database (ICSD); *Card No. 20-2242, Version 1.3.1*; FIZ Karlsruhe: Eggenstein-Leopoldshafen, 2003.
44. Zhang, W.; Zou, L.; Wang, L.; *Water Sci. Technol.* **2010**, *61*, 2863.
45. Rao, K. S. P.; Rao, M. V.; *Int. J. Eng. Sci. Res. Technol.* **2013**, *4*, 101.
46. Pandi, P.; Gopinathan, C.; Sakthivadivel, R.; Kavitha, M.; Karuppuchamy, M.; *Eng. Technol.* **2013**, *2*, 3237.
47. Zuas, O.; Hamim, N.; *Mater. Sci.* **2013**, *19*, 443.
48. Modine, N. A.; Armstrong, A. M.; Crawford, M. H.; Chow, W. W.; *J. Appl. Phys.* **2013**, *114*, 144.
49. Dozzi, M. V.; Sellì, E.; *J. Photochem. Photobiol. Rev.* **2013**, *14*, 13.
50. Yaithongkum, J.; Kooptarnond, K.; Sikong, L.; Kantachote, D.; *Adv. Mater. Res.* **2011**, *214*, 212.
51. Achoi, M. F.; Gambar, M. Z. M.; Rusop, M.; Abdullah, S.; *J. Phys.* **2013**, *431*, 2012.
52. Hema, M.; Arasi, A. Y.; Tamilselvi, P.; Anbarasan, R.; *Chem. Sci. Trans.* **2013**, *2*, 239.
53. Yeh, C. W.; Wu, K. R.; Hung, C. H.; Chang, H. C.; Hsu, C. J.; *Int. J. Photoenergy* **2012**, Article ID 285129.
54. Virkutyte, J.; Varma, R. S.; *RSC Adv.* **2012**, *2*, 1533.
55. Yu, J.; Xiong, J.; Cheng, B.; Liu, S.; *Appl. Catal., B* **2005**, *60*, 211.
56. Tian, Y.; Tatsuma, T.; *Chem. Commun.* **2004**, *16*, 1810.

57. Daniel, L. S.; Nagai, H.; Yoshida, N.; Sato, M.; *Catalysts* **2013**, *3*, 625.
58. Awazu, K.; Fujimaki, M.; Rockstuhl, C.; Tominaga, J.; Murakami, H.; Ohki, Y.; Yoshida, N.; Watanabe, T.; *J. Am. Chem. Soc.* **2008**, *130*, 1676.
59. Dall'Antonia, A. C.; Martins, M. A.; Moreno, R. M. B.; Mattoso, L. H. C.; Gonçalves, P. S.; Job, A. E.; *Polim.: Cienc. Tecnol.* **2009**, *19*, 63.
60. Estrada, M.; Reza, C.; Salmones, J.; Wang, J. A.; Manríquez, M. E.; Mora, J. M.; Hernández, M. L.; Zúñiga, A.; Contreras, J. L.; *J. New Mater. Electrochem. Syst.* **2014**, *17*, 23.
61. Li, Y.; Li, X.; Li, J.; Yin, J.; *Water Res.* **2006**, *40*, 1119.
62. Konstantinou, K.; Albanis, T. A.; *Appl. Catal., B* **2004**, *49*, 1.
63. Sabate, J.; Anderson, M. A.; Kikkawa, H.; Edwards, M.; Hill, C. G.; *J. Catal.* **1991**, *127*, 167.
64. Lu, M.; Pichat, P.; *Photocatalysis and Water Purification: from Fundamentals to Recent Applications: New Materials for Sustainable Energy and Development*; John Wiley & Sons: New York, 2013.
65. Atkins, P.; Paula, J.; *Physical Chemistry*, 8<sup>th</sup> ed.; Oxford: New York, 2006.

Submitted: April 8, 2015

Published online: November 5, 2015

FAPESP has sponsored the publication of this article.